Simulation and Microstructural Characterization of Zirconia/AA7020 Alloy Particle-Reinforced Metal Matrix Composites

[1]P. M. Jebaraj and A. Chennakesava Reddy[2]

[1]Professor, Department of Mechanical Engineering, Dr. Ambedkar Institute of Technology, Bangalore, India.
[2]Assistant Professor, Department of Mechanical Engineering, MJ College of Engineering and Technology, Hyderabad, India
dr_acreddy@yahoo.com

Abstract: *A hexagonal array unit cell/hexagonal ZrO_2 nanoparticle RVE models were used to predict micromechanical behavior and interfacial debonding in AA7020/ ZrO_2 composites. The AA7020/ ZrO_2 metal matrix composites were fabricated at 10%, 20% and 30% volume fractions of ZrO_2. AA7020/ ZrO_2 . The microstructure of AA7020 alloy/ ZrO_2 reveals the presence of porosity and partial agglomeration of ZrO_2 nanoparticles in the AA7020 alloy matrix. The interfacial debonding and matrix fracture were observed in the composites.*

Keywords: AA7020*, zirconia, hexagonal nanoparticle, RVE model, finite element analysis, debonding.*

1. INTRODUCTION

A major failure mode in composite structures is debonding. Bonding develops from physical or chemical interactions, interfacial frictional stress and thermal stresses due to mismatch between coefficient of thermal expansion of reinforcement and matrix. The understanding and control of the underlying interfacial phenomena governing the transmission of thermal, electrical, and mechanical properties across the whole composite might become of paramount importance when designing MMC for a particular task. A weak interface is desirable to enhance longitudinal strength and toughness, a strong interface is desirable to achieve good transverse properties. Surface roughness of the reinforcing material improves the mechanical interlocking at the interface, though the contribution of the resulting interfacial shear strength is secondary compared to chemical bonding [1]. A study was conducted on the silane interfacial effect on the fracture process of embedded single E-glass fiber [2]. The interfacial reinforcement reflects the progressed fracture rather than the instantaneous fracture. In a series of research, a variety of nanoparticles such as silicon nitride [3, 4], titanium oxide [5, 6], graphite [7], titanium carbide [8, 9], boron nitride [10], zirconium oxide [11], titanium nitride [12], titanium boride [13], zirconium carbide [14], silicon oxide [15], magnesium oxide [16] at 10%, 20% and 30% volume fractions were studied and the results computed from a unit cell with uniformly distributed particles were compared. The influence of progressive damage on stress-strain relation of particulate-reinforced composites was studied with two schemes. Finite element analysis for a unit cell containing one particle in a matrix was widely applied to fracture or debonding of particles [17]. The unit cell analysis has an advantage to provide details of damage process in one particle [3-16].

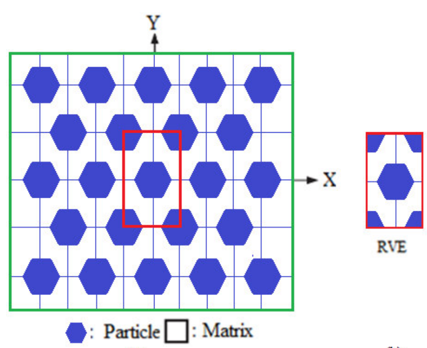

Figure 1: A hexagonal RVE containing an hexagonal nanoparticle.

Zirconia Powder (Zirconium Oxide, ZrO_2) is synthesized from zircon sand ($ZrO_2 \cdot SiO_2$) using a solid-state reaction process. Zirconia finds application in the manufacturing of valve components, wear and abrasion resistant components, bearings and cutting tools. In the present work, zirconia nanoparticles were reinforced in AA67020 alloy through the stir casting process. The effect of varying volume fractions of ZrO_2 on the microstructural and mechanical properties of AA7020 alloy is examined. The structure-property relationship is used to understand the observed mechanical behavior of the developed AA7020 alloy/ ZrO_2 composites. The shape of ZrO_2 nanoparticle considered in this work is a hexagonal. The periodic particle distribution was a hexagonal array as shown in figure 1.

2. THEORETICAL BACKGROUND

The strains along x- and y-directions can be determined as using the following equations:

$$\varepsilon_y = -\left(\frac{v_{xy}}{E_x} + \frac{1}{E_z}\right) P = \frac{\Delta y}{a} \quad (1)$$

$$\varepsilon_x = \left(\frac{1}{E_x} - \frac{1}{E_z}\right) P = \frac{\Delta x}{a} \quad (2)$$

The effective elastic moduli and Poisson's ratio in the transverse direction (xy-plane) as follows:

$$E_x = \frac{1}{\frac{\Delta x}{Pa} + \frac{1}{E_z}} \text{ and } E_y = \frac{1}{\frac{\Delta y}{Pa} + \frac{1}{E_z}} \quad (3)$$

$$v_{xy} = \left(\frac{\Delta y}{Pa} + \frac{1}{E_z}\right) / \left(\frac{\Delta x}{Pa} + \frac{1}{E_z}\right) \quad (4)$$

Once the change in lengths along x- and y- direction (Δx and Δy) are determined for the square RVE from the FEA, E_y and E_x and v_{xy} can be determined from Eqs. (3) and (4), correspondingly. Considering adhesion, formation of precipitates, particle size, agglomeration, voids/porosity, obstacles to the dislocation, and the interfacial reaction of the particle/matrix, the formula for the strength of composite is stated below:

$$\sigma_c = \left[\sigma_m \left\{\frac{1-(v_p+v_v)^{2/3}}{1-1.5(v_p+v_v)}\right\}\right] e^{m_p(v_p+v_v)} + kd_p^{-1/2} \quad (5)$$

$$k = E_m m_m / E_p m_p$$

where, v_v and v_p are the volume fractions of voids/porosity and nanoparticles in the composite respectively, m_p and m_m are the possion's ratios of the nanoparticles and matrix respectively, d_p is the mean nanoparticle size (diameter) and E_m and E_p is elastic moduli of the matrix and the particle respectively. Elastic modulus (Young's modulus) is a measure of the stiffness of a material and is a quantity used to characterize materials. Elastic modulus is the same in all orientations for isotropic materials. Anisotropy can be seen in many composites.

The upper-bound equation is given by

$$\frac{E_c}{E_m} = \left(\frac{1-v_v^{2/3}}{1-v_v^{2/3}+v_v}\right) + \frac{1+(\delta-1)v_p^{2/3}}{1+(\delta-1)(v_p^{2/3}-v_p)} \quad (6)$$

The lower-bound equation is given by

$$\frac{E_c}{E_m} = 1 + \frac{v_p - v_p}{\delta/(\delta-1)-(v_p+v_v)^{1/3}} \quad (7)$$

where, $\delta = E_p / E_m$.

The transverse modulus is given by

$$E_t = \frac{E_m E_p}{E_m + E_p(1-v_p^{2/3})/v_p^{2/3}} + E_m\left(1 - v_p^{2/3} - v_v^{2/3}\right) \quad (8)$$

3. MATERIALS METHODS

The matrix material was AA7020 alloy. The reinforcement material was ellipsoidal ZrO_2 nanoparticles of average size 100nm. The mechanical properties of materials used in the present work are given in table 1.

Table 1: Mechanical properties of AA7020 matrix and ZrO_2 nanoparticles

Property	AA7020	ZrO_2
Density, g/cc	2.78	6.15
Elastic modulus, GPa	72	250
Ultimate tensile strength, MPa	350	711
Poisson's ratio	0.33	0.32

AA7020 alloy/ ZrO_2 composites were manufactured by the stir casting process and low pressure casting technique with argon gas at 3.0 bar. The composite samples were give solution treatment and cold rolled to the predefined size of tensile specimens. The heat-treated samples were machined to get flat-rectangular specimens (figure 2) for the tensile tests. The tensile specimens were placed in the grips of a Universal Test Machine (UTM) at a specified grip separation and pulled until failure. The test speed was 2 mm/min. A strain gauge was used to determine elongation.

In this research, a cubical representative volume element (RVE) was implemented to analyze the tensile behavior AA7020/ ZrO_2 nanoparticle composites at three (10%, 20% and 30%) volume fractions of ZrO_2. The large strain PLANE183 element was used in the matrix in all the models. In order to model the adhesion between the matrix and the particle, a CONTACT 172 element was used.

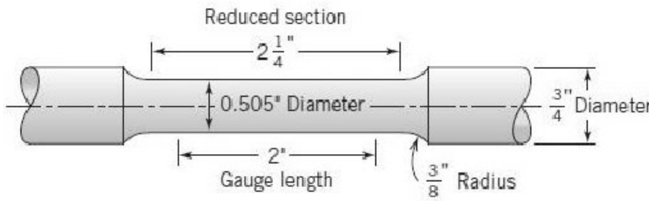

Figure 2: Shape and dimensions of tensile specimen

4. RESULTS AND DISCUSSION

The optical micrograph as shown in figure 3 reveals uniform distribution of ZrO_2 particles in AA7020 alloy matrix. The testes tensile specimens show no necking formation (figure 4). The fracture was at the centre doe a few specimens. The elongation of was decreased with increased volume fraction of ZrO_2 particles in AA7020 alloy matrix.

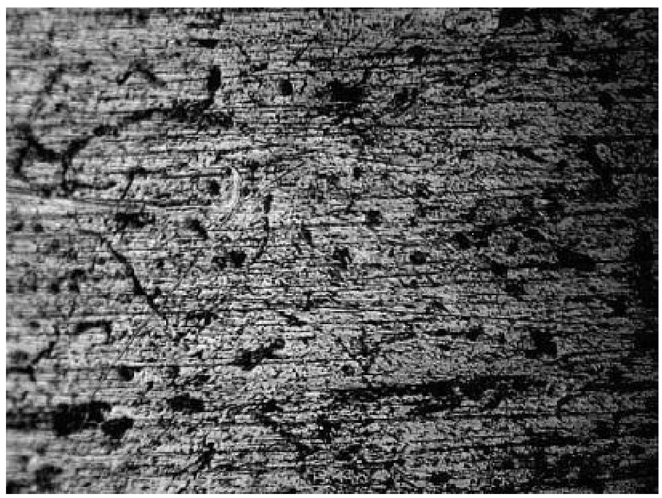

Figure 3: Optical micrograph showing uniform distribution of ZrO_2 nanoparticles.

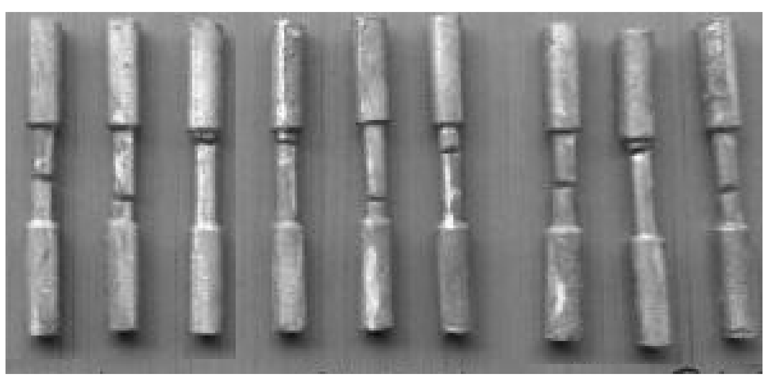

Figure 4: Tested tensile specimens.

4.1 Micromechanical Behavior

Figure 5a represents the normalized tensile strengths of the AA7020 alloy/ ZrO_2 composites obtained by FEA, present mathematical model, and experimental test. The tensile strength is normalized with ultimate tensile strength of AA7020 alloy. The results obtained from present mathematical model confirm the experimental results. The difference between the results obtained from experimental procedure and the FEA is due to the ignorance of porosity in the matrix and agglomeration of ZrO_2 particles. As seen in figure 5, the black matrix is aluminum and the white spots represent ZrO_2 nanoparticles. The grey area is silicon-rich interdendritic Al−Si eutectic. The phases are indicated by arrows on the images. It should be noted that ZrO_2 nanoparticles are uniformly dispersed in the matrix of AA7020 alloy and just a partial agglomeration in composites.

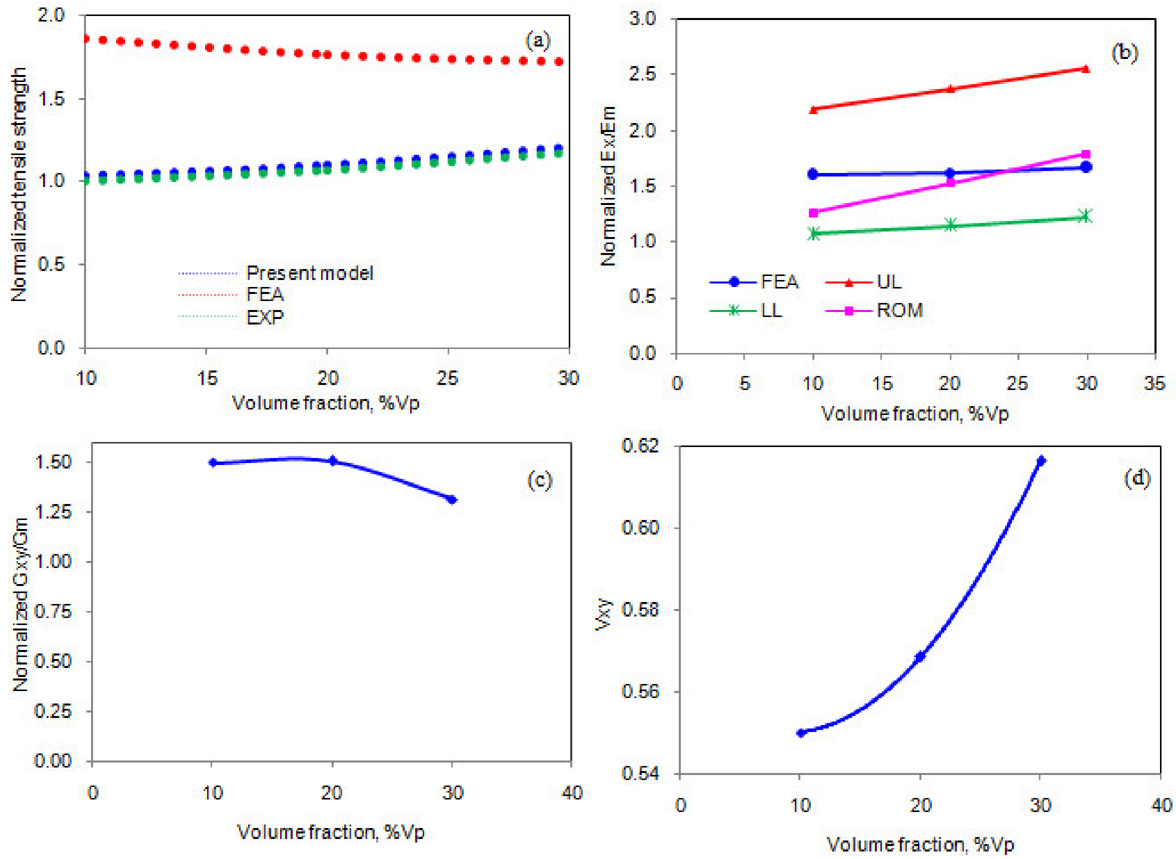

Figure 4: Effect of volume fraction on micromechanical behavior of AA7020/ ZrO_2 composites.

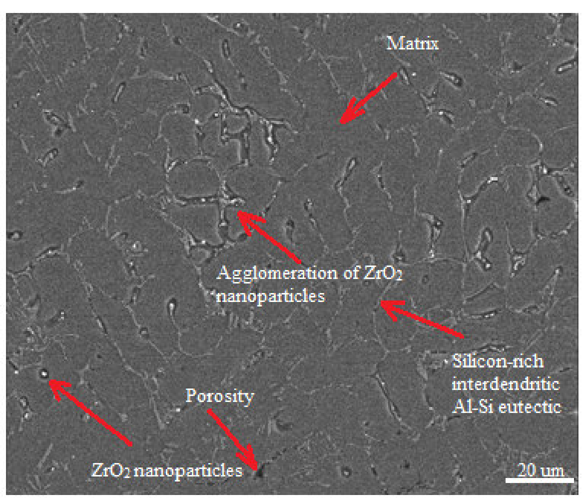

Figure 5: SEM image showing the agglomeration and porosity in AA7020/30% ZrO_2 composite.

The normalized elastic modulus is shown in figure 4b. The elastic modulus is normalized with the elastic modulus of AA7020 alloy. The stiffness of the composites increases with increase of volume fraction of ZrO_2. The upper limit (UL) values computed by the present mathematical model are higher than those values obtained by the 'Role of Mixtures (ROM)'and FEA. This is because of assumption of voids in the present mathematical model. The shear strength of the composites decreases with increase of volume fraction of ZrO_2 (figure 4c). The major Poisson's ratio increases with increase of volume fraction of ZrO_2 particles (figure 4d).

4.2 Fracture Analysis

If the particle deforms in an elastic manner (according to Hooke's law) then,

$$\tau = \frac{n}{2}\sigma_p \quad (9)$$

where σ_p is the particle stress. If particle fracture occurs when the stress in the particle reaches its ultimate tensile strength, $\sigma_{p,uts}$, then setting the boundary condition at

$$\sigma_p = \sigma_{p,\,uts} \quad (10)$$

The relationship between the strength of the particle and the interfacial shear stress is such that if

$$\sigma_{P,uts} < \frac{2\tau}{n} \quad (11)$$

Then the particle will fracture. From the figure 6b, it is observed that the ZrO_2 nanoparticle was not fractured as the condition in Eq. (11) is not satisfied. For the interfacial debonding/yielding to occur, the interfacial shear stress reaches its shear strength:

$$\tau = \tau_{max} \quad (12)$$

For particle/matrix interfacial debonding can occur if the following condition is satisfied:

$$\tau_{max} < \frac{n\sigma_p}{2} \quad (13)$$

It is observed from figure 6a that the interfacial debonding occurs between ZrO_2 nanoparticle and AA7020 alloy matrix as the condition in Eq.(13) is satisfied.

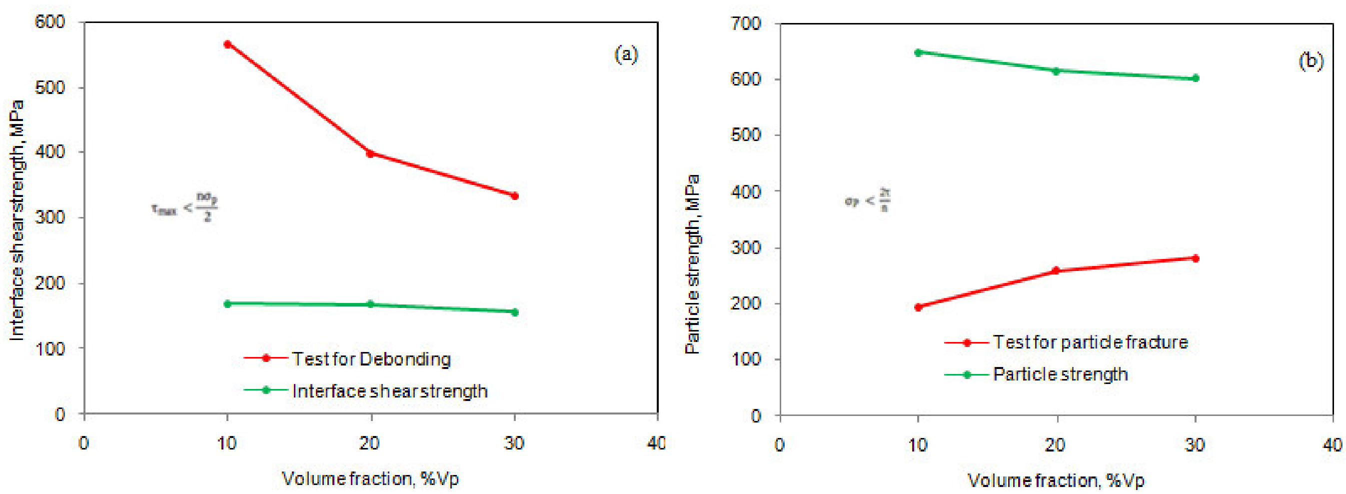

Figure 6: Criterion interfacial debonding (a) and for particle fracture (b).

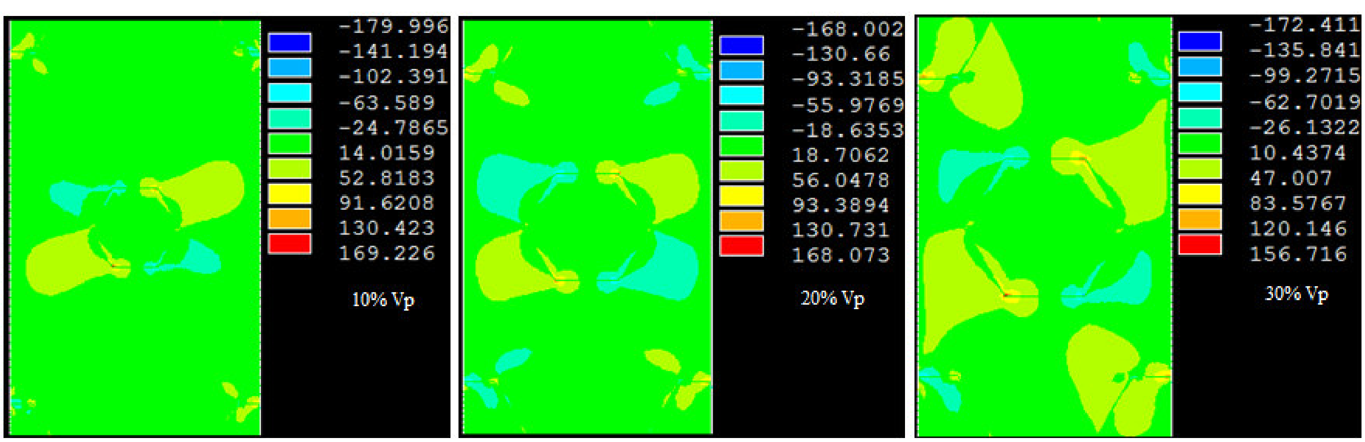

Figure 7: Images of tensile stress obtained from FEA.

As seen from figure 7 the shear stress developed at the interface are higher than that induced in the nanoparticle. Hence, the interfacial debonding was occurred between the particle and the matrix. The matrix fracture is also observed in AA7020/ ZrO_2 composites due to inadequate transfer of load from the matrix to the particle.

5. CONCLUSION

The microstructure of AA7020 alloy/ ZrO_2 reveals the presence of porosity and partial agglomeration of ZrO_2 nanoparticles in the AA7020 alloy matrix. FEA results are higher than those of experimentation due to ignorance of porosity and agglomeration during simulation. The shear stress is high at the interface leading to interfacial debonding in AA7020/ ZrO_2 composites. Due to lack of load transfer from the matrix to the particle, the fracture in the matrix is also observed.

REFERENCES

1. A. Mortensen, Interface chemistry of inorganic composite materials in 9th Riso international symposium on mechanical and physical behavior of metallic and ceramic composites, S. I. Anderson, H. Lilholt, O. B. Pedersen, pp.141-155 , Riso National Laboratory, Roskilde, Denmark, 1988.
2. B. Kotiveerachari, A. Chennakesava Reddy, Interfacial effect on the fracture mechanism in GFRP composites, CEMILAC Conference, Ministry of Defence, India, 20-21st August 1999.
3. A. Chennakesava Reddy, Assessment of Debonding and Particulate Fracture Occurrences in Circular Silicon Nitride Particulate/AA5050 Alloy Metal Matrix Composites , National Conference on Materials and Manufacturing Processes, Hyderabad, India, 27-28 February 1998, pp. 104-109.
4. A. Chennakesava Reddy, Evaluation of Debonding and Dislocation Occurrences in Rhombus Silicon Nitride Particulate/AA4015 Alloy Metal Matrix Composites, 1st National Conference on Modern Materials and Manufacturing , Pune, India, 19-20 December 1997, pp. 278-282.
5. S. Sundara Rajan, A. Chennakesava Reddy, Deformation Behavior of AA8090/ TiO_2 Nanoparticulate Reinforced Metal Matrix Composites with Debonding Interfaces, 2nd International Conference on Composite Materials and Characterization, Nagpur, India, 9-10 April 1999, pp. 245-248.
6. A. Chennakesava Reddy, Cohesive Zone Finite Element Analysis to Envisage Interface Debonding in AA7020/Titanium Oxide Nanoparticulate Metal Matrix Composites , 2nd International Conference on Composite Materials and Characterization, Nagpur, India, 9-10 April 1999, pp. 204-209.
7. A. Chennakesava Reddy, Micromechanical Modelling of Interfacial Debonding in AA1100/Graphite Nanoparticulate Reinforced Metal Matrix Composites, 2nd International Conference on Composite Materials and Characterization, Nagpur, India, 9-10 April 1999, pp. 249-253.
8. A. Chennakesava Reddy, Local Stress Differential for Particulate Fracture in AA2024/Titanium Carbide Nanoparticulate Metal Matrix Composites, National Conference on Materials and Manufacturing Processes, Hyderabad, India, 27-28 February 1998, pp. 127-131.
9. B. Kotiveera Chari, A. Chennakesava Reddy, Effect of Debonding on Overall Behavior of AA3003/Titanium Carbide Nanoparticulate Reinforced Metal Matrix Composites, 2nd International Conference on Composite Materials and Characterization, Nagpur, India, 9-10 April 1999, pp. 220-224.
10. H. B. Niranjan, A. Chennakesava Reddy, Effect of Particulate Debonding in AA5050/Boron Nitride Nanoparticulate Reinforced Metal Matrix Composites, 2nd International Conference on Composite Materials and Characterization, Nagpur, India, 9-10 April 1999, pp. 230-234.
11. P. M. Jebaraj, A. Chennakesava Reddy, Interface Debonding Prediction Technique for Tensile Loaded AA6061/Zirconium Oxide Nanoparticulate MMC, 2nd International Conference on Composite Materials and Characterization, Nagpur, India, 9-10 April 1999, pp. 235-239.
12. S. Sundara Rajan, A. Chennakesava Reddy, FEM Model for Volume Fraction Dependent Interface Debonding in TiN Nanoparticle Reinforced AA7020 Metal Matrix Composites, 2nd International Conference on Composite Materials and Characterization, Nagpur, India, 9-10 April 1999, pp. 240-244.
13. A. Chennakesava Reddy, Interfacial Debonding Analysis in Terms of Interfacial Tractions for Titanium Boride/AA3003 Alloy Metal Matrix Composites, 1st National Conference on Modern Materials and Manufacturing , Pune, India, 19-20 December 1997, pp. 124-127.
14. B. Kotiveera Chari, A. Chennakesava Reddy, Interfacial Debonding Analysis in Nanoparticulate Reinforced Metal Matrix Composites of AA8090/Zirconium Carbide, 2nd International Conference on Composite Materials and Characterization, Nagpur, India, 9-10 April 1999, pp. 210-214.
15. H. B. Niranjan, A. Chennakesava Reddy, Debonding Failure and Volume Fraction Effects in Nano-reinforced Composites of AA2024/Silicon Oxide, 2nd International Conference on Composite Materials and Characterization, Nagpur, India, 9-10 April 1999, pp. 215-219.

16. P. M. Jebaraj, A. Chennakesava Reddy, Analysis of Debonding along Interface of AA4015/Magnesium Oxide Nanoparticulate Reinforced Metal Matrix Composites, 2nd International Conference on Composite Materials and Characterization, Nagpur, India, 9-10 April 1999, pp. 225-229.
17. M. Finot, Y. L. Shen, A. Needleman, S. Suresh, Micromechanical modeling of reinforcement fracture in particle-reinforced metal-matrix composites, Metallurgical and Material Transaction, 25A, 1994, pp. 2403-2420.